

Enhancing Quality of Pose-varied Face Restoration with Local Weak Feature Sensing and GAN Prior

Kai Hu, *Student Member, IEEE* Yu Liu, Renhe Liu, Wei Lu*, Gang Yu, Bin Fu

Abstract—Facial semantic guidance (including facial landmarks, facial heatmaps, and facial parsing maps) and facial generative adversarial networks (GAN) prior have been widely used in blind face restoration (BFR) in recent years. Although existing BFR methods have achieved good performance in ordinary cases, these solutions have limited resilience when applied to face images with serious degradation and pose-varied (e.g., looking right, looking left, laughing, etc.) in real-world scenarios. In this work, we propose a well-designed blind face restoration network with generative facial prior. The proposed network is mainly comprised of an asymmetric codec and a StyleGAN2 prior network. In the asymmetric codec, we adopt a mixed multi-path residual block (MMRB) to gradually extract weak texture features of input images, which can better preserve the original facial features and avoid excessive fantasy. The MMRB can also be plug-and-play in other networks. Furthermore, thanks to the affluent and diverse facial priors of the StyleGAN2 model, we adopt a fine-tuned approach to flexibly restore natural and realistic facial details. Besides, a novel self-supervised training strategy is specially designed for face restoration tasks to fit the distribution closer to the target and maintain training stability. Extensive experiments on both synthetic and real-world datasets demonstrate that our model achieves superior performance to the prior art for face restoration and face super-resolution tasks.

Index Terms—Blind Face Restoration, StyleGAN2, Asymmetric Codec, Self-supervised Training.

I. INTRODUCTION

BLIND face restoration (BFR) is a typically ill-posed inverse problem and aims at reproducing realistic and reasonable high-quality (HQ) face images from unknown degraded inputs. Low-quality (LQ) face images are often affected by the combination of multiple unknown degradation factors in the wild, such as low resolution, noises, blur [1], and compression artifacts [2], etc.. Therefore, this may cause serious loss of high-frequency details in the image and affect the overall image quality. Furthermore, due to the complexity and diversity of facial postures, it is still a challenge to restore face images with natural and high-quality results for BFR tasks. The human face has a highly complex structure and has



Fig. 1. Restoration results from the old photos of the Solvay conference, 1927. Only some face images are displayed. Our method can restore the details of the original images to a large extent and avoid excessive fantasy. **Please zoom in for the best view.**

special properties different from other objects. Previous works based on Convolutional Neural Networks (CNN) and GAN use various facial semantic priors (including facial landmarks [3]–[5], facial parsing maps [1], [6]–[8], facial heatmaps [9], and facial component dictionaries [10]) to guide the networks to recover face shape and details. However, when these facial priors are adopted to restore severely degraded images, there is still much room for improvement in the restoration results due to the limited prior information.

As a generative facial model with excellent performance, StyleGAN [11]–[13] is capable of synthesizing face images with rich textures, changeable styles, and highly realistic vision, and providing rich and diverse priors, such as facial contours and textures of all areas (including hair, eyes, and mouth). So far, StyleGAN2 [12] has been widely applied to face restoration tasks, such as PULSE [14], pSp [7], PSFR-GAN [8], GFPGAN [15], GPEN [16], GCFSR [17], and Panini-Net [18]. However, although these methods have taken full advantage of the StyleGAN2 network or the pre-trained StyleGAN2 model, there is still limited resilience due to the lack of appropriate and efficient training strategies.

All in all, when used to restore the seriously degraded pose-varied face image, existing methods often have many problems in the output results, such as excessive fantasy, visual artifacts, blurry and unreasonable textures. To address this challenging problem, we propose a novel blind face restoration network with the GAN prior [12], composed of an asymmetric codec and a StyleGAN2 prior network. Firstly, since there are few weak texture features in degraded images, we propose a mixed multi-path residual block (MMRB), which mainly adopts a two-branch sparse structure to extract the features of different

Manuscript received xx; revised xx. This work was supported in part by Yunnan major science and technology special plan projects (202002AD080001), National Natural Science Foundation of China (61771338).

Kai Hu, Yu Liu, and Renhe Liu are with the School of Microelectronics, Tianjin University, Tianjin 3000072, China. Wei Lu is with the School of Electrical and Information, Tianjin University, Tianjin 3000072, China (e-mail: luwei@tju.edu.cn).

Gang Yu and Bin Fu are with GY-Lab, Tencent PCG.

Copyright © 2022 IEEE. Personal use of this material is permitted. However, permission to use this material for any other purposes must be obtained from the IEEE by sending an email to pubs-permissions@ieee.org.

scales and can achieve spatial interaction and aggregation of shared features through skip connections. In this work, we apply MMRB layers to gradually extract weak texture features of input images from shallow to deep.

Secondly, To better restore natural and high-quality face images, as shown in Fig. 1, we adopt the StyleGAN2 model with generative facial prior as the primary generator network and jointly fine-tune the generator with the codec. Using facial landmark points of training data, the position coordinates of the local areas are obtained, such as the eyes and mouth. We adopt then local facial losses to promote the authenticity of the output facial results during training. Finally, we introduce a training strategy of freezing a pre-trained discriminator (FreezeD), which helps our network recover more reasonable and high-fidelity results in complex degraded scenes. In particular, this training strategy helps our model to remain stable during training and speed up the fitting of the generated results to the target distribution.

Our main contributions are summarized as follows:

- We propose a well-designed blind face restoration network with generative facial prior, which can promote the quality of face images with complex facial posture and serious degradation.
- For the StyleGAN2 prior model, we specially design a novel self-supervised training strategy that freezes a pre-trained discriminator (FreezeD) and jointly fine-tunes the generator with the codec. It helps our model recover high-quality face images more realistically and reasonably and maintain stability during training.
- To better extract few and weak texture features in low-quality images, we propose a MMRB layer, which adopts a two-branch sparse structure to extract the features of different scales and can achieve spatial interaction and aggregation of shared features through skip connections.
- Our method achieves state-of-the-art results on multiple datasets. It can observe that our method can tackle seriously degraded face images in diverse poses and expressions and can restore more realistic and natural facial textures.

II. RELATED WORK

A. Face Restoration

For blind face restoration in the real world, the restoration problem becomes more complex due to the particularity of the face image itself and the influence of many unknown degradation factors, such as compression artifacts, low resolution, blur, and noise. There are three main research trends [19] for this task: basic CNN-based methods, GAN-based methods, and Prior-guided methods.

Basic CNN-based methods. IPFH [20] utilized deep reinforcement learning and facial illuminator to restore high-quality textures of human face. DPDFN [21] proposed a simple dual-path deep fusion network for face super-resolution without additional face priors, which constructed two individual branches for learning global facial contours and local face details and then fused the results of the two branches. Chen et al. [22] adopted a nearest neighbor network to model the

neighbor relationship in HR to produce high-quality and high-resolution outputs.

GAN-based methods. HiFaceGAN [23] proposed a collaborative suppression and replenishment framework to tackle unconstrained face restoration problems. TDAE [24] presented a discriminative generative network, which is not affected by posture and facial expression and can ultra-resolve low-resolution face images. Super-FAN [9] first proposed an end-to-end model that addresses face super-resolution and alignment via integrating a sub-network for face alignment through heat map regression and optimizing a heatmap loss. In order to improve the accuracy of face recognition, MDFR [25] proposed a multi-degradation face restoration model which can restore a given low-quality face to the high-quality one in arbitrary poses. PSFR-GAN [8] based on the StyleGAN2 network proposed a semantic-aware style transfer approach to modulate the features of different scales and recover HQ face details progressively. GCFSR [17] proposed a generative and controllable face super-resolution model without reliance on any additional priors, which can use to reconstruct faithful images with promising identity information. However, face restoration methods based on CNN and GAN have limited resilience due to lacking generative facial prior.

GAN Prior-guided methods. The pre-trained model based on the StyleGAN2 [12] is often used to solve the GAN inversion problem, such as face restoration and face super-resolution. PULSE [14] adopted a self-supervised training method to iteratively optimize the latent codes of StyleGAN2 model until the distance between outputs and inputs was below a threshold to restore high-quality facial images. pSp [7] utilized the pre-trained StyleGAN2 model and used a standard feature pyramid as an encoder network to solve image-to-image translation tasks. GFPGAN [15] also used the pre-trained StyleGAN2 model as a generative facial prior and then proposed channel-split spatial feature transform layers to perform spatial modulation on a split of features to improve the quality of face images. GPEN [16] directly embedded GAN prior into the codec structure as the decoder and jointly fine-tuned the GAN prior network with the deep neural network. Panini-Net [18] proposed a learnable mask to dynamically fuse the encoder's features with the features generated by GAN blocks in the pre-trained StyleGAN2 model and adopted a contrastive learning strategy [26] to extract discriminative degradation representations for degraded images. Although HQ face images can be restored using the GAN prior, their restoration results are not realistic enough for the face images with multiple poses and serious degradation.

B. Transferring GAN Priors

Transferring GAN prior model is also regarded as a domain adaptation, which mainly adjusts the data distribution of the pre-trained model to a domain suitable for other tasks [27]–[31]. For the pre-trained model, common strategies are to fine-tune or fix the parameters of the pre-trained model [14], [19], [32]. However, directly using GAN priors for training cannot reduce the difference between the two data distributions and improve the restored image quality [33]. Therefore, it

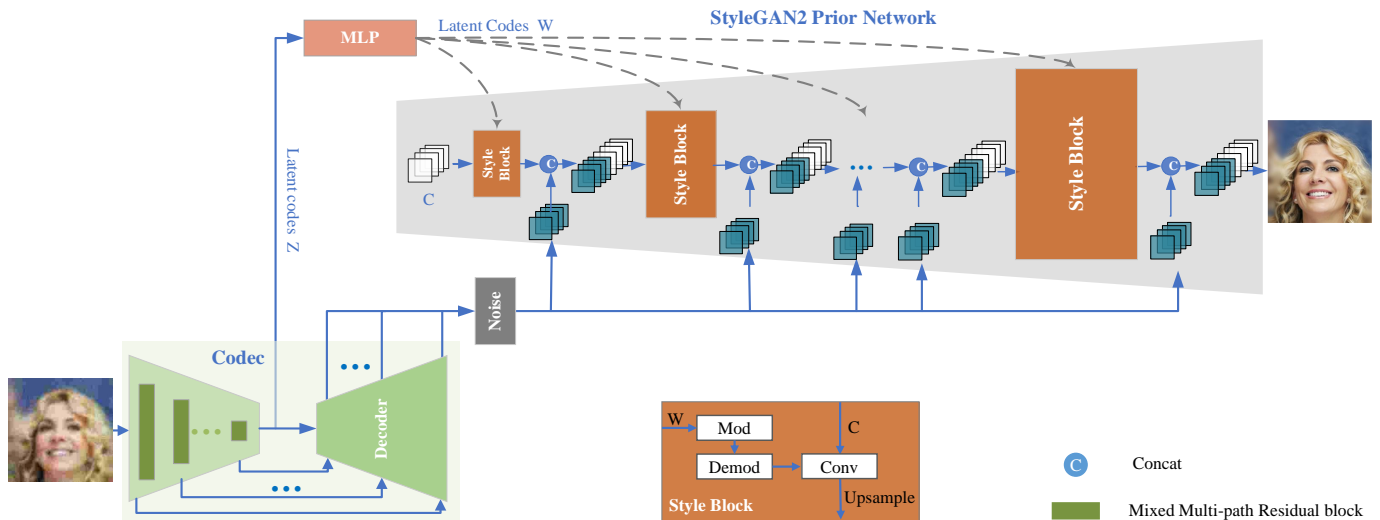


Fig. 2. The framework of our proposed method. It is mainly composed of an asymmetric codec and a StyleGAN2 prior network. The MMRB layer is adopted to gradually extract weak texture features of input images in the encoder. Furthermore, the inputs of the GAN prior network include latent codes \mathbf{W} , a learned constant feature tensor \mathbf{C} and noise branches. This prior network can then apply style blocks to gradually restore high-quality face images from coarse to fine.

needs to adopt appropriate training strategies, especially for seriously degraded image restoration tasks. Most relevant to our work, domain adaptation methods ([34]–[36]) built upon the StyleGAN [11] [12] demonstrate impressive visual quality and semantic interpretability in the target domain. StyleGAN-ADA [30] proposed an adaptive discriminator augmentation method to train the StyleGAN network on limited data samples. Mo et al. [37] froze lower layers of the discriminator to achieve domain adaptation and demonstrated the effectiveness of this simple baseline using various architectures and datasets. Huang et al. [32] proposed an Image-to-Image translation method that generates a new model in the target domain via a series of model transformations on the pre-trained StyleGAN2 model in the source domain.

C. Feature Extraction Block

So far, various feature extraction blocks have been proposed to improve the learning ability of convolution layers in a network. Multiple versions of inception blocks [38] [39] adopted parallel multi-scale convolution in the network to replace the dense structure, and fused all convolution results, and used the bottleneck layer for dimensionality reduction to reduce the amount of network computing. Kim et al. [40] added a short connection to the previous convolution layer and put forward the idea of residual learning, which can effectively alleviate the disappearance of gradients during training and reduce the number of parameters. After that, Zhang et al. [41] mainly increased the width of convolution by using the information compensation of other feature channels, which can reduce the vanishing gradient, realize the efficient utilization of feature information. Li et al. [42] motivated by the inception module proposed a multi-scale residual block to exploit the features of images at different scales. Inspired by the above methods, we propose a mixed multi-path residual block (MMRB) to extract image features of different paths and realize mixed interaction

between features to provide better modeling capabilities for face restoration.

III. OUR PROPOSED METHODS

A. Global Architecture

In this section, we will describe the well-designed network framework in Fig. 2, which can be used to solve a serious ill-posed inverse problem in the wild. The framework is inspired by StyleGAN [11], GFPGAN [15], and GPEN [16] models, consisting of an asymmetric codec and a StyleGAN2 prior network. Firstly, We input a low-quality image x into the codec, in which the encoder has one more MMRB layer in each scale than the decoder. That is because the encoder needs to provide more natural and reliable face latent features for the generator. The MMRB layer proposed by us can better extract the weak and few texture features in the degraded images. The input image x is then mapped to the closest latent codes \mathbf{Z} in the StyleGAN2 by the encoder. It can be seen from the StyleGAN [11] and StyleGAN2 [12] that images can be generated only by latent codes without noise branches, but the generated results lack rich and real texture information. Aiming to balance the fidelity and authenticity of the restoration results, we use the decoder and skip connections to reconstruct the multi-scale downsampled features, and directly output the reconstructed features at each level to the noise branches in the StyleGAN2. This process also benefits from the different practices of GFPGAN [15] and GPEN [16] networks. We have also verified the function of this process during training and have found that the reconstructed image has richer and more reasonable facial textures. Finally, to reduce the influence of degradation factors, we use L1 restoration loss similar to [15] for each resolution scale of the reconstructed image in the decoder. Finally, the process of codec is formulated by :

$$\hat{x}, \mathbf{Z} = \text{Codec}(x), \quad (1)$$

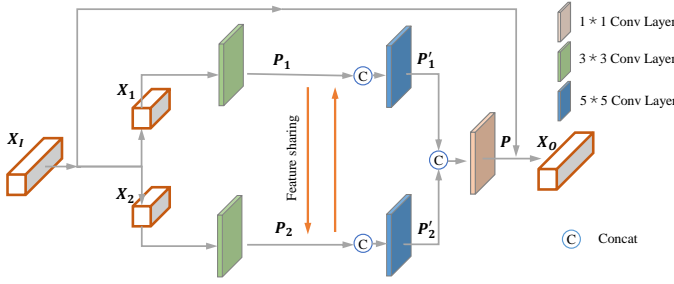


Fig. 3. Overview of the mixed multi-path residual block (MMRB).

Secondly, latent codes \mathbf{W} , a learned constant feature tensor \mathbf{C} and noise features \hat{x} are input into the pre-trained StyleGAN2, where \mathbf{W} are latent codes decoupled by the latent codes \mathbf{Z} through a mapping network of several multi-layer perceptron layers (MLP). Decoupling feature space is formulated by:

$$\mathbf{W} = \text{MLP}(\mathbf{Z}), \quad (2)$$

The \mathbf{W} ($w \in \mathbf{W}$) are then broadcasted to each style block, in which the Mod and Demod indicate the modulation and demodulation operation of latent codes \mathbf{W} , respectively. In particular, the input noises \hat{x} and the output \hat{y} of the style block after feature modulation are fused by concatenating rather than directly adding to convolutions in the StyleGAN2 model, which can take advantage of the features introduced by noise branches to flexibly restore the texture of local areas.

$$\mathbf{y}_{i+1} = \text{Style}(\mathbf{w}, \mathbf{y}_i, \text{Concat}[\hat{x}_i, \hat{y}_i]). \quad (3)$$

The output feature maps \mathbf{y} will be input to the next style block. On the basis of the fine-tuned training skills, we can apply style blocks to gradually restore high-quality face images from coarse to fine.

B. Mixed Multi-path Residual block

To extract slight and weak high-frequency textures in the degraded image, we propose a mixed multi-path residual block (MMRB). Here we will clearly describe its structure in Fig. 3. We design a two-branch and interactive feature extraction network, unlike previous works [38], [39], [41], [42]. We first equally split the input multi-channel feature maps \mathbf{X}_I rather than reduce dimensionality using a 1×1 bottleneck layer, which can reduce the parameters of convolution calculation for each branch.

$$\mathbf{X}_1, \mathbf{X}_2 = \text{Split}(\mathbf{X}_I), \quad (4)$$

Where $\text{Split}(\cdot)$ represents the separation operation of the feature maps in the channel dimension. $\mathbf{X}_I \in \mathbb{R}^{H \times W \times C}$. $\mathbf{X}_1, \mathbf{X}_2 \in \mathbb{R}^{H \times W \times C/2}$. We adopt then the two-branch sparse structure to extract the features of different scales. In order to improve the utilization of different scale features, skip connections are applied to share extracted features and achieve spatial interaction and aggregation of different features. The detailed definitions are as follows:

$$\mathbf{P}_1 = \mathbf{F}_1(\mathbf{X}_1, \mathbf{W}_1) = \sigma(\mathbf{W}_1(\mathbf{X}_1)), \quad (5)$$

$$\mathbf{P}_2 = \mathbf{F}_2(\mathbf{X}_2, \mathbf{W}_2) = \sigma(\mathbf{W}_2(\mathbf{X}_2)), \quad (6)$$

$$\mathbf{P}'_1 = \mathbf{F}_1(\mathbf{C}_1, \mathbf{W}_1) = \sigma(\mathbf{W}_1(\text{Concat}[\mathbf{P}_1, \mathbf{P}_2])), \quad (7)$$

$$\mathbf{P}'_2 = \mathbf{F}_2(\mathbf{C}_1, \mathbf{W}_2) = \sigma(\mathbf{W}_2(\text{Concat}[\mathbf{P}_1, \mathbf{P}_2])), \quad (8)$$

$$\mathbf{P} = \mathbf{F}_3(\mathbf{C}_2, \mathbf{W}_3) = \sigma\left(\mathbf{W}_3\left(\text{Concat}\left[\mathbf{P}'_1, \mathbf{P}'_2\right]\right)\right), \quad (9)$$

Where $\mathbf{F}(\cdot, \cdot)$ represents convolution mapping functions. $\sigma(\cdot)$ stands for the PReLU nonlinear activation function [43]. $\mathbf{W}_1, \mathbf{W}_2, \mathbf{W}_3$ indicate that the convolution kernel size used in the convolution layer are 3, 5 and 1, respectively. $\text{Concat}[\cdot, \cdot]$ denotes the concatenation operation. Finally, through the dimensionality reduction of 1×1 bottleneck layer, the output feature parameters are significantly reduced.

In order to make the block more efficient and practical, we adopt residual learning similar to in ResNet [41] to each MMRB. Formally, we describe the MMRB layer as:

$$\mathbf{X}_O = \mathbf{X}_I + \mathbf{P}. \quad (10)$$

Where \mathbf{X}_O represents the MMRB's output. $\mathbf{P} \in \mathbb{R}^{H \times W \times C}$ and is the output of multi-path feature maps fusion. In practice, The MMRB layer is applied to the encoder level by level from shallow layer to deep layer to improve our network's performance. What is more, it introduces fewer parameters and can be plug-and-play to enhance the ability of feature extraction in other networks.

C. Freeze Discriminator

Thanks to the powerful generation ability of the StyleGAN2 [12] prior model, the generated face image is genuinely diversified in structure, texture, and color information. We use the StyleGAN2 model as a generative facial prior and adopt a jointly fine-tuning training strategy for the pre-trained StyleGAN2 and codec. Fine-tuning the pre-trained StyleGAN2 model can better fit the complex degraded multi-pose face data into the target distribution. While the source domain and target domain are the same in our work. To make the distribution generated results better consistent with the target distribution, we introduce a Freeze Discriminator (FreezeD) training skill [37] for the StyleGAN2 to better learn the target distribution by freezing the higher-resolution layers of the discriminator during the training process. We find that simply freezing the lower layers of the discriminator and only fine-tuning the upper layers performs surprisingly well, and the generator is more stable during training.

Where the pre-trained discriminator model comes from the training results published by [16], that is because it has a prior knowledge to distinguish high-quality images, and its target distribution for training is the same as ours. What's more, using the discriminator model and generator for joint fine-tuning can improve the quality of the overall image and speed up the training process.

D. Model Objectives

To jointly fine-tune our restoration model, we use the following loss functions: the adversarial loss, the reconstruction loss, and the identity preserving loss. The adversarial loss is composed of a global adversarial loss and multiple local adversarial losses, in which the global adversarial loss function is defined as

$$L_{adv-g} = \min_G \max_D \mathbb{E}_{(X)} \log \left(1 + \exp \left(-D \left(G \left(X' \right) \right) \right) \right) \quad (11)$$

Where X and X' denote the ground-truth image and the generated one, and G is the pre-trained StyleGAN2 for fine-tuning. D is the pre-trained discriminator model from [16] and adopt the FreezeD strategy during training.

We believe the StyleGAN2 [11] model incorporates geometric face priors for BFR tasks. Therefore, we introduce local facial losses to focus generated results on local patch distributions, such as eyes and mouth. By using these local losses, we can effectively distinguish the high-frequency features of local regions to generate more natural and vivid local contents. In particular, it can make our model better to solve the unreal problem of multi-pose face restoration in the wild.

We employ local discriminators for the left eye, right eye, and mouth. The facial regions of interest (ROI) first need to be cropped and aligned based on the 68 key points solved by the facial keypoints detection model [4] and Mask R-CNN [44]. For each region, we build upon the same discriminator network and employ different local losses for adversarial training. The local facial losses are defined as follows:

$$L_{adv-l} = \sum_{ROI} \mathbb{E}_{(X'_{ROI})} \left[\log \left(1 - D_{ROI} \left(X'_{ROI} \right) \right) \right] \quad (12)$$

$$L_{adv} = \lambda_g L_{adv-g} + \lambda_l L_{adv-l} \quad (13)$$

Where the cross-entropy loss function is used and D_{ROI} is the local discriminator for each region. λ_g and λ_l represent the loss weights of global adversarial loss and local adversarial losses, respectively. We differentiate the weight of the discriminators to force the generator to focus more on local regions rather than the whole image during training. Besides, we adopt the L1-norm loss and feature matching loss as content losses L_C :

$$L_C = \lambda_{l1} \left\| X - X' \right\|_1 + \lambda_{FM} \mathbb{E} \left[\sum_{i=1}^N \left\| \psi_i(X) - \psi_i(X') \right\|_2 \right], \quad (14)$$

λ_{l1} and λ_{FM} represent the loss weights of the L1-norm loss and feature matching loss [45]. Inspired by [46], we give λ_{FM} a very small value of the weight parameter to avoid generating smooth results and checkerboard artifacts. ψ_i indicates the i -th convolution layer of the pre-trained VGG network [47]. N is the total number of intermediate layers used for feature extraction. In order to enforce the restored face to have a small distance with the ground truth in the deep feature space, we introduce a face preserving loss [48]:

$$L_{FP} = \lambda_{FP} \left\| \phi(X) - \phi(X') \right\|_1. \quad (15)$$

Where λ_{FP} denotes the loss weight. ϕ represents the face feature extractor that adopts the pre-trained ArcFace [49] model for face recognition.

The overall loss optimization function used by our model is defined as

$$L_{total} = L_{adv} + L_C + L_{FP} \quad (16)$$

The loss hyper-parameters are set as follows: $\lambda_g = 0.5$, $\lambda_l = 3$, $\lambda_{l1} = 8$, $\lambda_{FM} = 0.02$, $\lambda_{FP} = 10$.

IV. EXPERIMENTS

A. Datasets

Training Datasets. We train on the 70k high-quality face images from the FFHQ dataset, which is synthesized by [12]. We resize the resolution of all images to 512×512 during training. To make the training data more in line with the degradation of the real scenes, we follow the practice in [50] [15] [16] and adopt the following degradation model with all possible degradation factors in the wild to synthesize LQ training data:

$$x = \mathbb{D}(y) = [(y \otimes k) \downarrow_s + n_\delta]_{JPEG_q} \quad (17)$$

\mathbb{D} denotes the degradation process for HQ images. The HQ face image y is first convolved \otimes with blur kernel k . Then, a downsampling operation with scale factor s is performed. Meanwhile, we continue to superimpose adding noise n on the high-quality image. Finally, the LQ image x is obtained by JPEG compression. To simulate the seriously degraded scenes, we randomly sample k , s , δ and q from 41, $[0.4 : 8]$, $[0 : 25]$, $[5 : 50]$ for each training pair in our experiments, respectively. In particular, we use Gaussian blur and motion blur to deal with the possible blur of the image in the natural scenes.

Testing Datasets. To better verify the performance of our model in complex degraded scenes, we use various types of low-quality datasets for testing, and they do not overlap with the training data. We make a brief description of these datasets.

1) *CelebA Data* is a synthetic dataset with 30000 high-quality face images [51]. We select 2556 face images with complex facial posture and degrade the selected images using the above degradation model and parameters.

2) *LFW Data* comes from [52] and is composed of more than 13k face pictures of famous people all over the world with different orientations, expressions, and lighting environments. They are real low-quality images with only a single face. The image size is 250 pixels \times 250 pixels. We select 1610 images with relatively low quality for testing.

3) *FDDB Data* comes from [53] and contains 5171 human faces in 2845 images taken from different natural scenes. The number of faces in the image is uncertain, not a single number. Moreover, the width and height of images are not equal, and the difference is noticeable. We select 1629 images with relatively low quality for testing.

4) *WebFace Data* is collected face images from the Internet by [54], including tens of thousands of images with a size of 250 pixels \times 250 pixels. They are real low-quality images with only a single face and have many old black-and-white photos. We select 804 images with relatively low quality for testing.

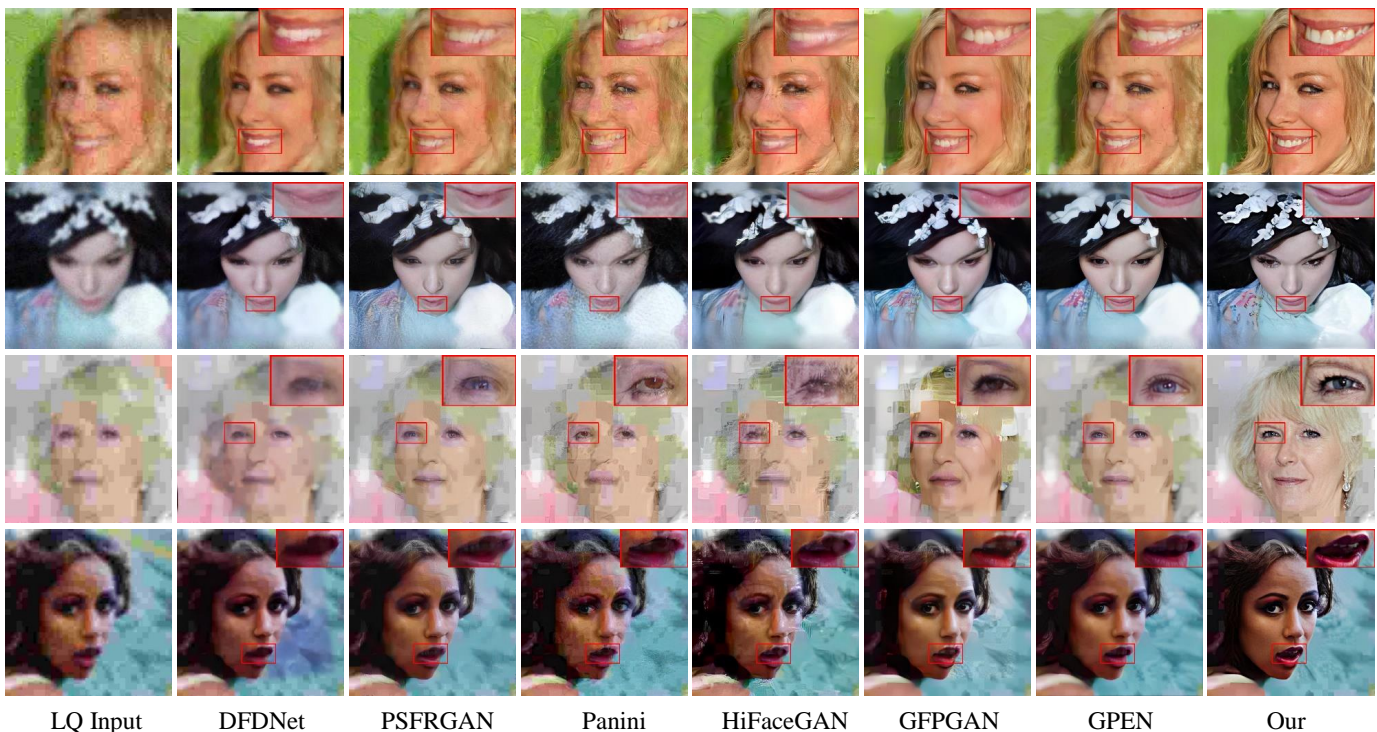


Fig. 4. Qualitative comparisons with several state-of-the-art face restoration methods on the CelebA Data. To intuitively feel the performance difference of each method, we enlarge and display local areas. **Zoom in for best view.**

B. Implementation Details and Evaluation Metrics

We adopt the FreezeD strategy [37] to the global discriminator from [16], and freeze the parameters of the first five convolution layers and fine-tune the remaining deep features. We then jointly fine-tune the Stylegan2 model retrained by [16] with the codec. The input image dimension mapped to the nearest latent codes is consistent with the pre-trained Stylegan2 model. At the same time, the resolution and dimension for the output feature maps of every level in the reconstruction process are consistent with the noise branch of the pre-trained model. For each MMRB layer, we adopt it layer by layer to extract weak texture features in low-quality images.

During the experiment, we train our model with Adam optimizer [55] and perform a total of 700k iterations with a batch size of 4. The learning rate (LR) varies for different parts, including the codec, the global discriminator, the local discriminator, the pre-trained Stylegan2 model, and noise branches. They are set to 2×10^{-3} , 2×10^{-5} , 2×10^{-3} , 2×10^{-4} and 2×10^{-3} , respectively. The local discriminator includes three facial components: left eye, right eye, and mouth. They use the same learning rate and discriminator model. Furthermore, a piece-wise attenuation strategy is adopted. We implement our model with the PyTorch framework and train it using two NVIDIA V100 GPUs.

For the evaluation, we employ a widely-used non-reference perceptual metric: NIQE [56]. Moreover, we also adopt pixel-wise metrics (PSNR and SSIM) and the reference perceptual metrics (LPIPS [57] and FID [58]) for the CelebA Data with Ground Truth (GT).

TABLE I
QUANTITATIVE COMPARISONS OF VARIOUS BFR METHODS ON CELEBA DATA. BOLD RED INDICATES THE BEST PERFORMANCE, AND BOLD BLUE INDICATES THE SECOND. REFERENCE EVALUATION METRICS ARE ADOPTED, SUCH AS PSNR, SSIM, LPIPS, AND FID, AND NON-REFERENCE PERCEPTUAL METRIC (NIQE) IS ALSO ADOPTED.

Methods	PSNR↑	SSIM↑	LPIPS↓	FID↓	NIQE ↓
HiFaceGAN [23]	24.506	0.612	0.196	31.545	4.427
DFDNet [10]	22.470	0.663	0.232	54.358	5.916
PSFRGAN [8]	24.884	0.663	0.192	34.695	4.765
Panini [18]	24.679	0.611	0.194	44.696	3.837
GPEN [16]	25.190	0.680	0.169	21.852	4.712
GFPGAN [15]	24.895	0.688	0.172	21.160	4.746
Our	26.034	0.702	0.162	16.080	4.285
GT	∞	1	0	2.478	4.188

C. Experiments on Synthetic Images

To better show the practicability and generality of our model, we verify the performance of face restoration and face super-resolution tasks through synthetic CelebA Data.

Face Restoration. To verify the superiority of the method mentioned in this paper, We make qualitative and quantitative comparisons with several of the latest blind face restoration methods, respectively, including DFDNet [10], PSFRGAN [8], Panini [18], HiFaceGAN [23], GFPGAN [15], and GPEN [16]. We also introduce metric values corresponding to the GT to understand better the difference between the test results of different methods and the GT in quantitative analyses.

The quantitative and qualitative results of different methods are shown in Tab. I and Fig. 4, respectively. Our method is optimal in all indicators and has the best performance according to the quantitative results. Although the NIQE metric is slightly lower than the best, it does not affect the priority

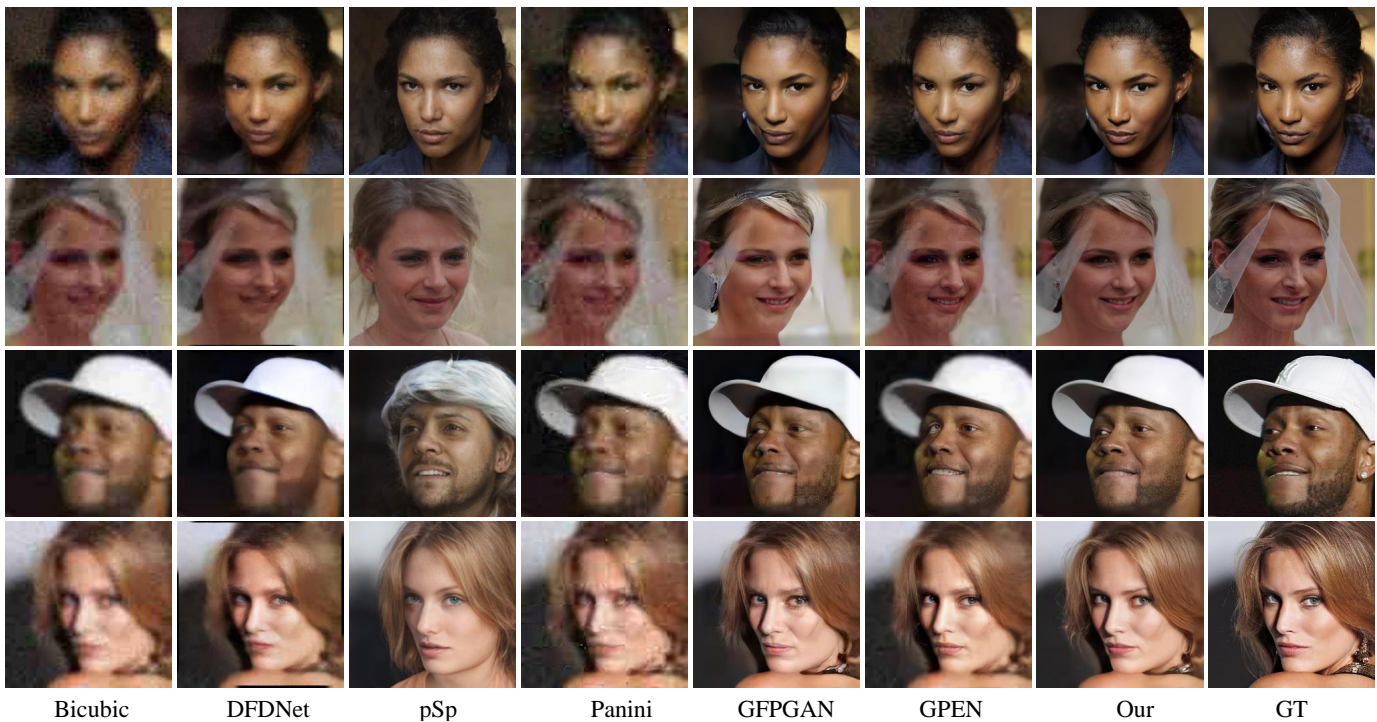


Fig. 5. Qualitative comparisons of 4x face super-resolution by different methods. We do not apply local magnification displays for the qualitative comparison results, which intends to view the differences between them in the form of the whole picture. **Zoom in for best view.**

of our method. That is because this perceptual metric can only roughly reflect the local difference between tested images in deep space and the learned perceptual features and can not better show the effectiveness of the recovery model [59]. What’s more, thanks to the fine-tuning training strategy, the visual qualitative comparison results show that our restoration images are more realistic and natural and have the best visual sensory effect, especially in the eyes and mouth areas. And our method can restore the complex degraded multi-pose face image more flexibly. In particular, the difference can be seen more clearly and intuitively by zooming in the local details. In addition, it is also seen that our method can improve the image quality of non-facial regions.

Face Super-resolution. We use the first 1500 images of CelebA Data and perform 4x downsampling of the input images to verify the super-resolution performance of different methods in the wild. Furthermore, we also make qualitative and quantitative comparisons with several state-of-the-art face super-resolution methods, including SuperFAN [9], pSp [7], Panini [18], HiFaceGAN [23], DFDNet [58], GFPGAN [15], and GPEN [16]. Our method needs to upsample tested images to the original scale and then input them into the network for testing.

The quantitative and qualitative results of different methods are shown in Tab. II and Fig. 5, respectively. As can be seen from the quantitative results, Our method can perform super-resolution on LQ images, and the output results are significantly better than other face super-resolution methods in all indicators. In particular, the output results of our model can be closer to the GT by using the MMRB layer, both in qualitative and quantitative results. We do not adopt local magnification

TABLE II
 QUANTITATIVE COMPARISONS OF VARIOUS FSR METHODS ON CELEBA DATA. WE ADOPT THE BICUBIC INTERPOLATION FOR 4X DOWN-SAMPLING OF THE INPUT DATA TO VERIFY THE SUPER-RESOLUTION PERFORMANCE OF DIFFERENT METHODS. BOLD RED INDICATES THE BEST PERFORMANCE, AND BOLD BLUE INDICATES SECOND ONE.

Methods	PSNR↑	SSIM↑	LPIPS↓	FID↓	NIQE ↓
Bicubic	23.757	0.641	0.297	148.468	10.460
SuperFAN [9]	23.193	0.617	0.290	152.188	7.857
pSp [7]	18.493	0.580	0.242	67.596	5.647
HiFaceGAN [23]	19.946	0.470	0.326	230.756	10.480
DFDNet [58]	21.772	0.638	0.260	93.107	6.416
Panini [18]	23.417	0.620	0.278	165.834	6.898
GPEN [16]	24.248	0.658	0.217	50.348	5.886
GFPGAN [15]	23.780	0.656	0.190	32.894	4.955
Our	24.797	0.674	0.189	27.403	4.449
GT	∞	1	0	2.413	4.036

displays for the qualitative comparison results, which intends to view the differences between them in the form of the whole picture. By visual comparison results, our results have fewer or less noticeable artifacts and texture blur, whether in facial texture, hair, or background. Although the pSp method [7] also shows promising results in the visualization effect, it is quite different from the GT due to its design idea.

D. Experiments on Images in the Wild

We evaluate our method on the FDDB Data, LFW Data, and WedFace Data, which are face images with complex facial poses in real scenes and suffer from multiple complex unknown degradations. To test the generalization ability, we make qualitative and quantitative comparisons with several latest blind face restoration methods, such as DFDNet [10],

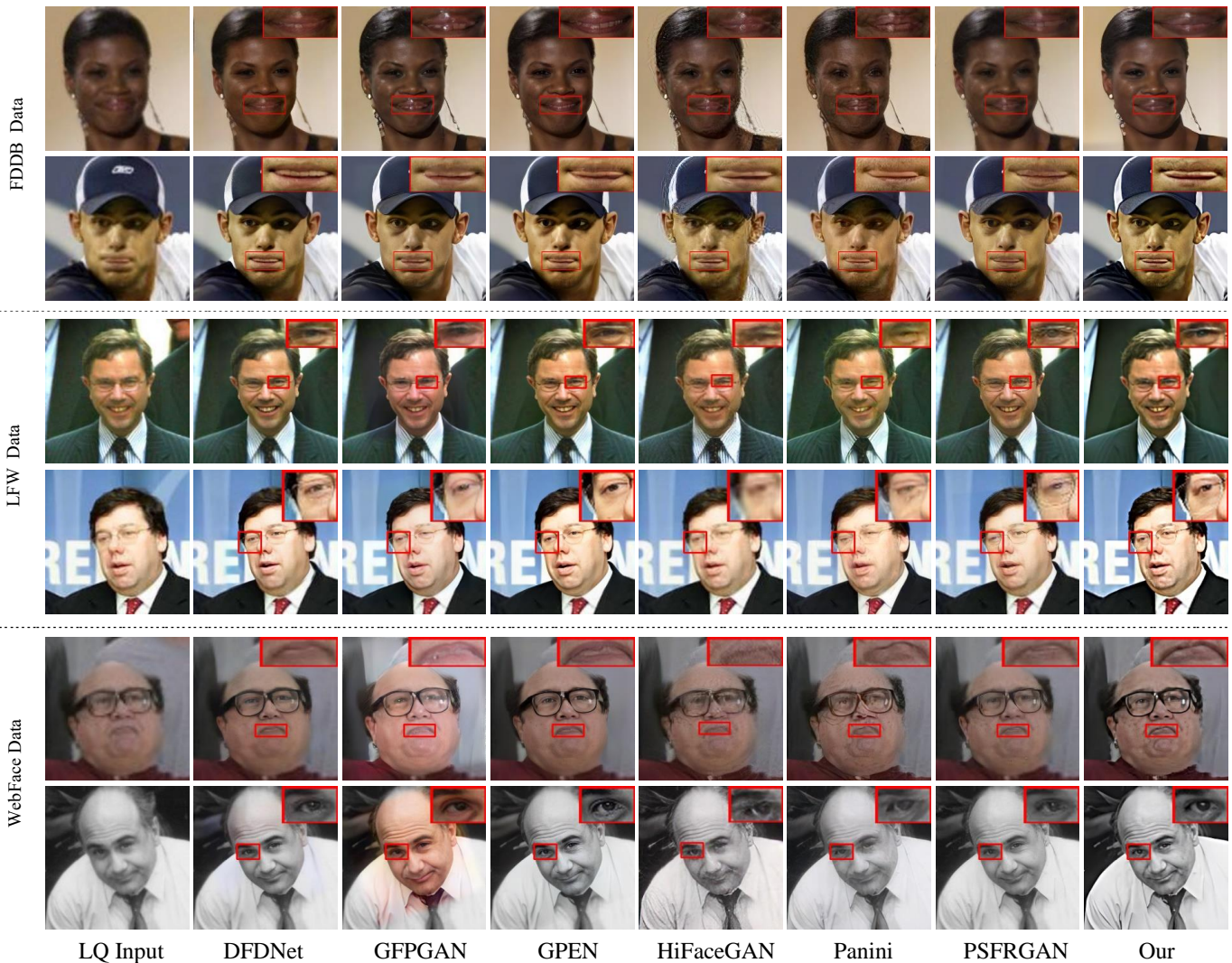


Fig. 6. Qualitative comparisons on the **FDDDB Data**, **LFW Data**, and **WebFace Data**. **Zoom in for best view**.

TABLE III

QUANTITATIVE COMPARISONS OF VARIOUS FSR METHODS IN THE WILD, SUCH AS **FDDB DATA**, **LFW DATA**, **WEBFACE DATA**. ONLY THE NON-REFERENCE PERCEPTUAL METRIC (NIQE) IS ADOPTED. “-” MEANS THAT THE RESULT IS UNAVAILABLE.

Dataset Methods	FDDB Data NIQE ↓	LFW Data NIQE ↓	WebFace Data NIQE ↓
Input	4.262	5.454	4.875
HiFaceGAN [23]	3.956	4.548	4.969
DFDNet [10]	4.153	4.990	5.449
PSFRGAN [8]	4.334	5.461	5.830
Panini [18]	—	4.694	4.605
GPEN [16]	4.110	5.418	5.793
GFPGAN [15]	4.009	4.982	5.313
Ours	3.578	4.548	4.875

PSFRGAN [8], Panini [18], HiFaceGAN [23], GFPGAN [15], and GPEN [16]. Since there is no GT in the real degraded image, we adopt the non-reference perceptual metric (NIQE) to test the performance of different methods. For the FDDB data, in order to facilitate qualitative comparison, we select some images and utilize the pre-trained RetinaFace face detection model [60] to cut out a single face with consistent width and height for testing.

The quantitative and qualitative results are presented in Tab. III and Fig. 6. It can be seen that our method still has prominent leadership in quantitative indicators and visualization results. Thanks to our careful design model and the excellent training strategy, the restored images have more apparent facial texture, more comfortable color information, and higher visual quality. In particular, the local components in the face are more realistic and reasonable. Although the numerical value is not the best on WebFace Data, it is evident from the visual effect that our method still has excellent performance. In the quantitative comparison, Panini method [18] lacks tested results on the FDDB Data, mainly because the images in the dataset have the problem of unequal width and height. What’s more, this method strictly requires equal width and height of the input images.

E. Ablation Studies

To better understand the roles of different components and training strategies in our method, we train them separately and apply qualitative and quantitative comparisons to test the

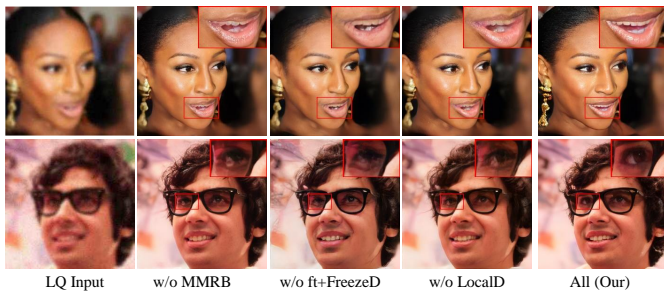


Fig. 7. Comparative results of different variables in our model. **Zoom in for best view.**

TABLE IV

QUANTITATIVE COMPARISONS OF DIFFERENT VARIANTS ON CELEBA DATA. BOLD BLACK INDICATES THE BEST PERFORMANCE.

Components	PSNR \uparrow	SSIM \uparrow	LPIPS \downarrow	FID \downarrow	NIQE \downarrow
a) w/o MMRB	25.977	0.699	0.163	17.027	4.682
b) w/o LocalID	26.010	0.697	0.163	16.908	4.614
c) w/o ft+FreezeD	25.704	0.692	0.171	19.543	4.546
All (Our)	26.034	0.702	0.162	16.080	4.285

performance. The involved relevant variables are as follows: without MMRB layer (w/o MMRB), without Local Discriminator (w/o LocalID), and without the fine-tuning and Freeze Discriminator strategy (w/o ft+FreezeD). As can be seen from the Fig. 7 and Tab. IV, we can find that:

MMRB layer. If the MMRB layer in the encoder is adopted, it can better maintain the original features of the input image and avoid the excessive illusion of local contents. However, when we remove the MMRB layers, it can find that the textures of the restored results are not complete, and the authenticity is weakened, especially in local areas.

Local Discriminator. if the network lacks local discriminators and the constraint of local facial losses during training, the restoration results are not natural enough and complete, and the visual sense is poor. That is mainly because the eyes and mouth significantly impact the overall quality.

Fine-tuning and FreezeD strategy. This training strategy significantly impacts the restoration results of our model, whether whether it is the qualitative or quantitative comparisons. It can also greatly reduce the distribution difference between the restoration results and the target domain and fit the real high fidelity face images better. However, if the training strategy is not adopted, we can find that it has the worst value of all metrics, and the visualization results are also the worst.

V. CONCLUSION

Aiming at the problem that complex degraded pose-varied and multi-expression face images are challenging to restore, we meticulously designed a restoration network with a generative facial prior for BFR tasks. To better preserve the original facial features and avoid excessive fantasy, we exploited MMRB layers to gradually extract weak texture features in the input images. Furthermore, we fine-tuned the pre-trained StyleGAN2 model and adopted the FreezeD strategy for the global discriminator model, which can better fit the distribution of diverse face images suitable for the natural scenes and improve the quality of the overall images. And especially,

because eyes and mouth regions are difficult to recover, we adopted different local adversarial losses to constrain our model for these regions to realistically restore face images. Extensive experiments on synthetic and multiple real-world datasets demonstrated that our model can restore complex degraded pose-varied face images and outperform the latest optimal BFR methods. The restoration results have richer textures, more natural details, and better visual sense. Most importantly, our method can also promote the image quality of non-facial regions and can restore old photos, and film and television works. And it can also be applied to other tasks such as face super-resolution.

REFERENCES

- [1] Z. Shen, W.-S. Lai, T. Xu, J. Kautz, and M.-H. Yang, "Deep semantic face deblurring," in *Proc. IEEE Conf. Comput. Vis. Pattern Recognit. (CVPR)*, 2018, pp. 8260–8269.
- [2] C. Dong, Y. Deng, C. C. Loy, and X. Tang, "Compression artifacts reduction by a deep convolutional network," in *Proc. IEEE Conf. Comput. Vis. Pattern Recognit. (CVPR)*, 2015, pp. 576–584.
- [3] M. Jeong, B. C. Ko, S. Kwak, and J.-Y. Nam, "Driver facial landmark detection in real driving situations," *IEEE Trans. Circuits Syst. Video Technol.*, vol. 28, no. 10, pp. 2753–2767, 2017.
- [4] H. Jin, S. Liao, and L. Shao, "Pixel-in-pixel net: Towards efficient facial landmark detection in the wild," *Int. J. Comput. Vis.*, vol. 129, no. 12, pp. 3174–3194, 2021.
- [5] S. Sharma and V. Kumar, "3d landmark-based face restoration for recognition using variational autoencoder and triplet loss," *IET Biom.*, vol. 10, no. 1, pp. 87–98, 2021.
- [6] Y. Chen, Y. Tai, X. Liu, C. Shen, and J. Yang, "Fsrnet: End-to-end learning face super-resolution with facial priors," in *Proc. IEEE Conf. Comput. Vis. Pattern Recognit. (CVPR)*, 2018, pp. 2492–2501.
- [7] E. Richardson, Y. Alaluf, O. Patashnik, Y. Nitzan, Y. Azar, S. Shapiro, and D. Cohen-Or, "Encoding in style: a stylegan encoder for image-to-image translation," in *Proc. IEEE Conf. Comput. Vis. Pattern Recognit. (CVPR)*, 2021, pp. 2287–2296.
- [8] C. Chen, X. Li, L. Yang, X. Lin, L. Zhang, and K.-Y. K. Wong, "Progressive semantic-aware style transformation for blind face restoration," in *Proc. IEEE Conf. Comput. Vis. Pattern Recognit. (CVPR)*, 2021, pp. 11 896–11 905.
- [9] A. Bulat and G. Tzimiropoulos, "Super-fan: Integrated facial landmark localization and super-resolution of real-world low resolution faces in arbitrary poses with gans," in *Proc. IEEE Conf. Comput. Vis. Pattern Recognit. (CVPR)*, 2018, pp. 109–117.
- [10] X. Li, C. Chen, S. Zhou, X. Lin, W. Zuo, and L. Zhang, "Blind face restoration via deep multi-scale component dictionaries," in *Proc. Comput. Vis. (ECCV)*. Springer, 2020, pp. 399–415.
- [11] T. Karras, S. Laine, and T. Aila, "A style-based generator architecture for generative adversarial networks," in *Proc. IEEE Conf. Comput. Vis. Pattern Recognit. (CVPR)*, 2019, pp. 4401–4410.
- [12] T. Karras, S. Laine, M. Aittala, J. Hellsten, J. Lehtinen, and T. Aila, "Analyzing and improving the image quality of stylegan," in *Proc. IEEE Conf. Comput. Vis. Pattern Recognit. (CVPR)*, 2020, pp. 8110–8119.
- [13] T. Karras, M. Aittala, S. Laine, E. Härkönen, J. Hellsten, J. Lehtinen, and T. Aila, "Alias-free generative adversarial networks," *Proc. Adv. Neural Inf. Process. Syst. (NeurIPS)*, vol. 34, 2021.
- [14] S. Menon, A. Damian, S. Hu, N. Ravi, and C. Rudin, "Pulse: Self-supervised photo upsampling via latent space exploration of generative models," in *Proc. IEEE Conf. Comput. Vis. Pattern Recognit. (CVPR)*, 2020, pp. 2437–2445.
- [15] X. Wang, Y. Li, H. Zhang, and Y. Shan, "Towards real-world blind face restoration with generative facial prior," in *Proc. IEEE Conf. Comput. Vis. Pattern Recognit. (CVPR)*, 2021, pp. 9168–9178.
- [16] T. Yang, P. Ren, X. Xie, and L. Zhang, "Gan prior embedded network for blind face restoration in the wild," in *Proc. IEEE Conf. Comput. Vis. Pattern Recognit. (CVPR)*, 2021, pp. 672–681.
- [17] J. He, W. Shi, K. Chen, L. Fu, and C. Dong, "Gcfsr: a generative and controllable face super resolution method without facial and gan priors," 2022, *arXiv:2203.07319*. [Online]. Available: <https://arxiv.org/abs/2203.07319>.

- [18] Y. Wang, Y. Hu, and J. Zhang, "Panini-net: Gan prior based degradation-aware feature interpolation for face restoration," 2022, *arXiv:2203.08444*. [Online]. Available: <https://arxiv.org/abs/2203.08444>.
- [19] J. Jiang, C. Wang, X. Liu, and J. Ma, "Deep learning-based face super-resolution: A survey," *ACM Comput. Surv.*, vol. 55, no. 1, pp. 1–36, 2021.
- [20] X. Cheng, J. Lu, B. Yuan, and J. Zhou, "Identity-preserving face hallucination via deep reinforcement learning," *IEEE Trans. Circuits Syst. Video Technol.*, vol. 30, no. 12, pp. 4796–4809, 2019.
- [21] K. Jiang, Z. Wang, P. Yi, T. Lu, J. Jiang, and Z. Xiong, "Dual-path deep fusion network for face image hallucination," *IEEE Trans. Neural Networks Learn. Syst.*, 2020.
- [22] L. Chen, J. Pan, R. Hu, Z. Han, C. Liang, and Y. Wu, "Modeling and optimizing of the multi-layer nearest neighbor network for face image super-resolution," *IEEE Trans. Circuits Syst. Video Technol.*, vol. 30, no. 12, pp. 4513–4525, 2019.
- [23] L. Yang, S. Wang, S. Ma, W. Gao, C. Liu, P. Wang, and P. Ren, "Hifacegan: Face renovation via collaborative suppression and replenishment," in *Proc. ACM Multimedia Conf. (MM)*, 2020, pp. 1551–1560.
- [24] X. Yu and F. Porikli, "Hallucinating very low-resolution unaligned and noisy face images by transformative discriminative autoencoders," in *Proc. IEEE Conf. Comput. Vis. Pattern Recognit. (CVPR)*, 2017, pp. 3760–3768.
- [25] X. Tu, J. Zhao, Q. Liu, W. Ai, G. Guo, Z. Li, W. Liu, and J. Feng, "Joint face restoration and frontalization for recognition," *IEEE Trans. Circuits Syst. Video Technol.*, vol. 32, no. 3, pp. 1285–1298, 2021.
- [26] R. Liu, Y. Ge, C. L. Choi, X. Wang, and H. Li, "Divco: Diverse conditional image synthesis via contrastive generative adversarial network," in *Proc. IEEE Conf. Comput. Vis. Pattern Recognit. (CVPR)*, 2021, pp. 16 377–16 386.
- [27] C. Zhang and Q. Zhao, "Deep discriminative domain adaptation," *Inf. Sci.*, vol. 575, pp. 599–610, 2021.
- [28] M. Zhang and Q. Ling, "Supervised pixel-wise gan for face super-resolution," *IEEE Trans. Multimedia*, vol. 23, pp. 1938–1950, 2020.
- [29] K. Zhou, Z. Liu, Y. Qiao, T. Xiang, and C. C. Loy, "Domain generalization in vision: A survey," 2021, *arXiv:2103.02503*. [Online]. Available: <https://arxiv.org/abs/2103.02503>.
- [30] T. Karras, M. Aittala, J. Hellsten, S. Laine, J. Lehtinen, and T. Aila, "Training generative adversarial networks with limited data," *Proc. Adv. Neural Inf. Process. Syst. (NeurIPS)*, vol. 33, pp. 12 104–12 114, 2020.
- [31] W. Zhuang, X. Gan, Y. Wen, X. Zhang, S. Zhang, and S. Yi, "Towards unsupervised domain adaptation for deep face recognition under privacy constraints via federated learning," 2021, *arXiv:2105.07606*. [Online]. Available: <https://arxiv.org/abs/2105.07606>.
- [32] J. Huang, J. Liao, and S. Kwong, "Unsupervised image-to-image translation via pre-trained stylegan2 network," *IEEE Trans. Multimedia*, vol. 24, pp. 1435–1448, 2021.
- [33] J. Back, "Fine-tuning stylegan2 for cartoon face generation," 2021, *arXiv:2106.12445*. [Online]. Available: <https://arxiv.org/abs/2106.12445>.
- [34] P. Zhu, R. Abdal, J. Femiani, and P. Wonka, "Mind the gap: Domain gap control for single shot domain adaptation for generative adversarial networks," 2021, *arXiv:2110.08398*. [Online]. Available: <https://arxiv.org/abs/2110.08398>.
- [35] O. Tov, Y. Alaluf, Y. Nitzan, O. Patashnik, and D. Cohen-Or, "Designing an encoder for stylegan image manipulation," *ACM Trans. Graph.*, vol. 40, no. 4, pp. 1–14, 2021.
- [36] G. Song, L. Luo, J. Liu, W.-C. Ma, C. Lai, C. Zheng, and T.-J. Cham, "Agilegan: stylizing portraits by inversion-consistent transfer learning," *ACM Trans. Graph.*, vol. 40, no. 4, pp. 1–13, 2021.
- [37] S. Mo, M. Cho, and J. Shin, "Freeze the discriminator: a simple baseline for fine-tuning gans," 2020, *arXiv:2002.10964*. [Online]. Available: <https://arxiv.org/abs/2002.10964>.
- [38] C. Szegedy, W. Liu, Y. Jia, P. Sermanet, S. Reed, D. Anguelov, D. Erhan, V. Vanhoucke, and A. Rabinovich, "Going deeper with convolutions," in *Proc. IEEE Conf. Comput. Vis. Pattern Recognit. (CVPR)*, 2015, pp. 1–9.
- [39] C. Szegedy, S. Ioffe, V. Vanhoucke, and A. A. Alemi, "Inception-v4, inception-resnet and the impact of residual connections on learning," in *Proc. AAAI Conf. Artif. Intell. (AAAI)*, 2017.
- [40] K. He, X. Zhang, S. Ren, and J. Sun, "Deep residual learning for image recognition," in *Proc. IEEE Conf. Comput. Vis. Pattern Recognit. (CVPR)*, 2016, pp. 770–778.
- [41] Y. Zhang, Y. Tian, Y. Kong, B. Zhong, and Y. Fu, "Residual dense network for image super-resolution," in *Proc. IEEE Conf. Comput. Vis. Pattern Recognit. (CVPR)*, 2018, pp. 2472–2481.
- [42] J. Li, F. Fang, K. Mei, and G. Zhang, "Multi-scale residual network for image super-resolution," in *Proc. Eur. Conf. Comput. Vis. (ECCV)*, 2018, pp. 517–532.
- [43] K. He, X. Zhang, S. Ren, and J. Sun, "Delving deep into rectifiers: Surpassing human-level performance on imagenet classification," in *Proc. IEEE Int. Conf. Comput. Vis. (ICCV)*, 2015, pp. 1026–1034.
- [44] K. He, G. Gkioxari, P. Dollár, and R. Girshick, "Mask r-cnn," in *Proc. IEEE Conf. Comput. Vis. Pattern Recognit. (CVPR)*, 2017, pp. 2961–2969.
- [45] T.-C. Wang, M.-Y. Liu, J.-Y. Zhu, A. Tao, J. Kautz, and B. Catanzaro, "High-resolution image synthesis and semantic manipulation with conditional gans," in *Proc. IEEE Conf. Comput. Vis. Pattern Recognit. (CVPR)*, 2018, pp. 8798–8807.
- [46] H. Zhao, O. Gallo, I. Frosio, and J. Kautz, "Loss functions for image restoration with neural networks," *IEEE Trans. Comput. Imaging*, vol. 3, no. 1, pp. 47–57, 2016.
- [47] K. Simonyan and A. Zisserman, "Very deep convolutional networks for large-scale image recognition," 2014, *arXiv:1409.1556*. [Online]. Available: <https://arxiv.org/abs/1409.1556>.
- [48] R. Huang, S. Zhang, T. Li, and R. He, "Beyond face rotation: Global and local perception gan for photorealistic and identity preserving frontal view synthesis," in *Proc. IEEE Int. Conf. Comput. Vis. (ICCV)*, 2017, pp. 2439–2448.
- [49] D. Jiankang, G. Jia, Z. Yuxiang, Y. Jinke, K. Irene, and Z. Stefanos, "Retinaface: Single-stage dense face localisation in the wild," 2019, *arXiv:1905.00641*. [Online]. Available: <https://arxiv.org/abs/1905.00641>.
- [50] X. Wang, L. Xie, C. Dong, and Y. Shan, "Real-esrgan: Training real-world blind super-resolution with pure synthetic data," in *Proc. IEEE Conf. Comput. Vis. Pattern Recognit. (CVPR)*, 2021, pp. 1905–1914.
- [51] Z. Liu, P. Luo, X. Wang, and X. Tang, "Deep learning face attributes in the wild," in *Proc. IEEE Int. Conf. Comput. Vis. (ICCV)*, 2015, pp. 3730–3738.
- [52] G. B. Huang, M. Mattar, T. Berg, and E. Learned-Miller, "Labeled faces in the wild: A database for studying face recognition in unconstrained environments," in *Workshop on faces in 'Real-Life' Images: detection, alignment, and recognition*, 2008.
- [53] V. Jain and E. Learned-Miller, "Fddb: A benchmark for face detection in unconstrained settings," University of Massachusetts, Amherst, Tech. Rep. UM-CS-2010-009, 2010.
- [54] D. Yi, Z. Lei, S. Liao, and S. Z. Li, "Learning face representation from scratch," 2014, *arXiv:1411.7923*. [Online]. Available: <https://arxiv.org/abs/1411.7923>.
- [55] D. P. Kingma and J. Ba, "Adam: A method for stochastic optimization," 2014, *arXiv:1412.6980*. [Online]. Available: <https://arxiv.org/abs/1412.6980>.
- [56] A. Mittal, R. Soundararajan, and A. C. Bovik, "Making a "completely blind" image quality analyzer," *IEEE Signal Process. Lett.*, vol. 20, no. 3, pp. 209–212, 2012.
- [57] R. Zhang, P. Isola, A. A. Efros, E. Shechtman, and O. Wang, "The unreasonable effectiveness of deep features as a perceptual metric," in *Proc. IEEE Conf. Comput. Vis. Pattern Recognit. (CVPR)*, 2018, pp. 586–595.
- [58] M. Heusel, H. Ramsauer, T. Unterthiner, B. Nessler, and S. Hochreiter, "Gans trained by a two time-scale update rule converge to a local nash equilibrium," *Proc. Adv. Neural Inf. Process. Syst. (NeurIPS)*, vol. 30, 2017.
- [59] Y. Blau, R. Mechrez, R. Timofte, T. Michaeli, and L. Zelnik-Manor, "The 2018 pirm challenge on perceptual image super-resolution," in *Proc. Eur. Conf. Comput. Vis. Workshops (ECCVW)*, 2018, pp. 0–0.
- [60] J. Deng, J. Guo, E. Verivas, I. Kotsia, and S. Zafeiriou, "Retinaface: Single-shot multi-level face localisation in the wild," in *Proc. IEEE Conf. Comput. Vis. Pattern Recognit. (CVPR)*, 2020, pp. 5203–5212.



Kai Hu received the B.S. degree in optoelectronic information science and engineering from North University of China, Taiyuan, in 2017, and the M.S. degree in electronic and communication engineering from Tianjin University, Tianjin, in 2021, where he is currently pursuing the Ph.D. degree. His research interests include image/video processing and computer vision.



Bin Fu is a director at Tencent. He leads the development and research team for GY-Lab. His research results have been widely used in Tencent products like QQ.



Yu Liu (M'06) received his BEng in electronic engineering from Tianjin University, Tianjin, China, in 1998. From 1998 to 2000, he worked as an electronic engineer in Shenzhen, China. In 2000, he returned to Tianjin University and received his MEng in information and communication engineering and Ph.D. in signal and information processing both from Tianjin University in 2002 and 2005, respectively. Currently, he is a full professor with the School of Microelectronics, Tianjin University.

From 2011 to 2012, Dr. Liu was a visiting research fellow with the Department of Electrical Engineering, Princeton University, Princeton, NJ, USA. His research interests include sensing and applications in multimedia signal processing, compressed sensing, and machine intelligence.



Renhe Liu received his B.S. degree in communication engineering from Guangxi University, Nanning, China, in 2016, and he is currently working towards a Ph.D. degree at the School of Microelectronic, Tianjin University, Tianjin, China. His research interests include multimedia signal and image processing.



Wei Lu received his B.Eng. degree in Electronic Engineering, and Ph.D. degree in signal and information processing from Tianjin University, Tianjin, China, in 1998 and 2003 respectively. He is currently an associate professor in the School of Electrical Engineering, Tianjin University. His teaching and research interests include digital image processing, pattern recognition and embedded systems.



Gang Yu is a research leader at Tencent. He received Ph.D. from Nanyang Technological University (NTU), Singapore. Before joining Tencent, he was the team leader in Megvii, leading the development of detection/segmentation techniques for mobile and embedded devices. He has published more than 30 papers in top journals and conferences. He is the winner for more than ten challenges, including COCO detection/skeleton (2017 & 2018), Widerface Face Detection (2018), ActivityNet AVA Detection (2018), and WAD Instance Segmentation

(2018). He received Microsoft Research Asia Fellowship in 2011.